


Cyclic deformation behavior of Mg–SiC nanocomposites on the macroscale and nanoscale

Daniela Hübler^{1,2}  | Kai Winkler³ | Ralf Riedel⁴ | Sepideh Kamrani¹ | Claudia Fleck¹

¹Chair of Materials Science & Engineering, Institute of Technology Berlin, Berlin, Germany

²Division Tribology and Wear Protection, Bundesanstalt für Materialforschung und -prüfung, Berlin, Germany

³Theoretical Biophysics, Institute for Biology, Humboldt University Berlin, Berlin, Germany

⁴Fachgebiet Disperse Feststoffe, Fachbereich Material- und Geowissenschaften, Technische Universität Darmstadt, Darmstadt, Germany

Correspondence

Daniela Hübler and Claudia Fleck, Chair of Materials Science & Engineering, Institute of Technology Berlin, Straße des 17. Juni 135, 10623 Berlin, Germany.
Email: huebler@tu-berlin.de; claudia.fleck@tu-berlin.de

Funding information

Deutsche Forschungsgemeinschaft

Abstract

Metal-ceramic nanocomposites are promising candidates for applications necessitating light weight and excellent fatigue resistance. We produced Mg–SiC nanocomposites from mechanically milled powders, yielding a homogeneous nanocrystalline structure and excellent quasistatic strength values. Little is known, however, about the fatigue behavior of such composites. Here, we used load increase tests on the macroscale to yield estimation values of the fatigue endurance limit. Fatigue strength increased significantly for the materials processed by the powder metallurgical route. We further investigated the cyclic deformation behavior under stress-controlled conditions on the macroscale and nanoscale. Cyclic nanoindentation showed that indentation depth and cyclic plastic deformation decreased with increasing reinforcement content, hinting to a higher cyclic strength and corroborating the results from the macroscopic load increase tests. Our results therefore show that cyclic nanoindentation reliably determines the plastic deformation behavior of Mg nanocomposites offering the possibility of fast material analysis.

KEYWORDS

cyclic deformation behavior, cyclic nanoindentation, fatigue behavior, load increase test, Mg–SiC nanocomposite

1 | INTRODUCTION

There is increasing need for lightweight materials capable of sustaining cyclic loading over a long lifetime, specifically in the vehicle or aviation industry. Designing such materials requires thorough understanding of the fatigue behavior and cyclic deformation behavior.¹ Metal-matrix composites (MMCs) offer a promising way to

combine low weight with high strength and ductility, also for cyclic loading conditions. In MMCs reinforced with micron-sized SiC particles, interface debonding and/or particle cracking are the predominant failure mechanisms, both under quasistatic and fatigue loading.^{2,3} Fatigue resistance of MMCs depends on many parameters, comprising grain size, reinforcement geometry, and distribution as well as coherence between reinforcements and matrix. The use of nanoparticles in MMCs has high potential to promote excellent interfacial bonding, and

Sepideh Kamrani and Claudia Fleck contributed equally to the paper.

This is an open access article under the terms of the Creative Commons Attribution License, which permits use, distribution and reproduction in any medium, provided the original work is properly cited.

© 2021 The Authors. *Fatigue & Fracture of Engineering Materials & Structures* published by John Wiley & Sons Ltd.

thus excellent load-bearing capability.^{4–7} Importantly, regarding fatigue resistance, nanoparticles promote strain hardening within nanocomposites as well during processing as during service loading. This leads to a higher density of pre-existing dislocations with beneficial dislocation-nanoparticle as well as dislocation-dislocation interactions.⁸ One consequence is the activation of nonbasal slip systems in the Mg matrix, which can lead to improved fracture strains.^{2,9}

To provide local information on cyclic plastic zone, cyclic hardening, and crack propagation, nanoindentation has been suggested.¹⁰ The method gives insights into dynamic processes within a material that lead to both dislocation generation and annihilation due to the effective applied stress, and distribution of internal stresses. So far only one study reports on the nanofatigue behavior of a Mg alloy using nanoindentation. Loading was, however, limited to 300 cycles.¹¹ Schmahl et al.¹² presented nanofatigue experiments on an Al–Si–Mg alloy with loading up to a much higher cycle number of 10^5 .

In contrast to cyclic nanoindentation, a large number of macrofatigue tests has been published for Mg alloy composites, for example, Hassan et al.,⁸ including Mg alloy–SiC composites,^{13,14} and pure Mg nanocomposites.^{3,15–19} On the macro level, constant amplitude (CAT) and load increase tests (LIT) are often used to investigate the complex processes during fatigue loading. Specifically, LIT are useful for estimating the fatigue endurance limit and cyclic stress strain curves, when only a small number of samples is available as previously shown for a variety of materials, also for Mg alloys.^{20,21} While endurance limits of about 60 MPa (CAT, 2×10^6 cycles)¹⁰ and 71 MPa (CAT, 1.2×10^6 cycles) have been reported for pure Mg and AZ31, respectively, reinforcement of AZ31 by Al₂O₃ nanoparticles improved the fatigue endurance limit to 91 MPa.¹⁸ Therefore, an increase in endurance limit can also be assumed for pure-Mg-nanocomposites. To the best of our knowledge, there are no studies on the macro-fatigue behavior of Mg–SiC nanocomposites.

Here, we report on high-cycle nanofatigue and macrofatigue tests on a Mg–SiC MMC made from mechanically milled composite powders with nanoscale reinforcements. Nanofatigue tests were performed up to cycle numbers of 10^5 and analyzed using the method proposed previously for Al alloys.¹² Fatigue mechanisms were investigated by observations of fracture surfaces of macrofatigued samples, and texture analysis was deployed to support our conclusions on the active deformation mechanisms. Comparisons of the plastic deformation behavior on the nanoscale and macroscale helped us

to evaluate to what extent cyclic nanoindentation tests can be used to predict the macrofatigue behavior.

2 | MATERIALS AND METHODS

2.1 | Sample preparation

Mg–SiC nanocomposites with SiC nanoparticles with volume fractions of 1 vol% and 3 vol% were produced by high-energy mechanical milling, cold-isostatic pressing, sintering, and hot extrusion. Mg powder with an average particle size of -325 mesh and β -SiC powder with an average particle size of 50 nm were used. Further details of the processing are given in Penther et al.²² We previously showed^{22,23} that this processing route leads to a homogeneous distribution of the nanoparticles in the matrix and to a very fine grain that is retained throughout all processing steps. Henceforth, these nanocomposites are referred to as M1S_n and M3S_n for samples with reinforcement contents of 1 or 3 vol% SiC nanoparticles, respectively. Mechanically milled pure Mg (MM) and nonmilled pure Mg (Mg) were used as reference materials. One nanoindentation specimen was cut off from each extruded flat rod with dimensions of 15×2 mm. The cross-sections were then ground stepwise with SiC paper down to 4000 grit using ethanol as lubricant, and subsequently polished, using ethanol and diamond spray down to a particle size of $\frac{1}{4}$ μ m. Three fatigue specimens of each composition were extracted from as-extruded flat rods, cut parallel to the extrusion direction (ED) by wire electrical discharge machining (EDM; AGIECUT AC Vertex 1 F, GF Machining Solutions GmbH, Geneva, Switzerland). The geometry and size of the specimens is shown in Figure 1. In order to remove the oxide layer and the EDM-induced damage, thus preventing stress raising effects during testing, the sample surfaces were stepwise polished using diamond spray down to 1- μ m particle size (Struers, Ballerup, Denmark). We may safely assume a surface roughness in the range of about 1 μ m as bigger scratches were excluded by light microscopic inspection.

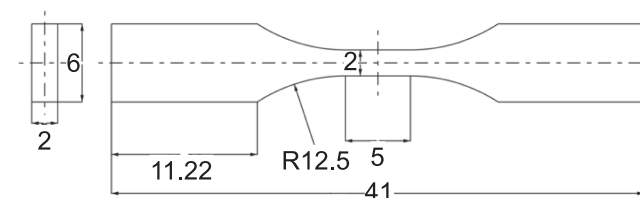


FIGURE 1 Geometry of the fatigue specimens

2.2 | Mechanical testing

2.2.1 | Nanofatigue behavior

For local fatigue analysis, cyclic nanoindentation was performed with a Hysitron TI 950 TriboIndenter (Bruker Corporation, Billerica, Massachusetts, USA) equipped with a standard Berkovich diamond indenter tip. High-frequency “loading” cycles ($f = 201$ Hz) were combined with interspersed low-frequency “measurement” cycles ($f = 0.05$ Hz) as described in detail elsewhere¹² at maximum and minimum loads of 968 and 72 μN , respectively. Note that, in compliance with the usual notation in nanoindentation, the loads are given as positive values even though they are compressive loads. The maximum number of cycles was 10.⁵ Several areas of each sample were cyclically indented with a grid arrangement of 4×5 indents, with all indents in a grid 10 μm apart from each other

The hysteresis data of at least 20 indents per sample were evaluated by custom-made code. The calculated parameters were averaged over all indents, resulting in average-value-curves. To analyze the plastic deformation behavior, we evaluated the changes in D_{\min} during cyclic loading. Because slight differences in the applied force could not be avoided ($\sim 9\%$ in P_{\min}), D_{\min} were normalized by the corresponding P_{\min} :

$$\Delta(D_{\min}/P_{\min}) = (D_{\min}/P_{\min})(N_{x+1}) - (D_{\min}/P_{\min})(N_x) \quad (1)$$

with D_{\min} the minimum displacement at minimum load P_{\min} and N_x and N_{x+1} the number of cycles in consecutive measurement cycles, indicated by subscripts “ x ” and “ $x+1$ ”. Because the number of cycles between measurement cycles was not constant, $\Delta(D_{\min}/P_{\min})$ was normalized by the number of cycles between consecutive measurement cycles:

$$\Delta D_{\min\text{-norm}} = \Delta(D_{\min}/P_{\min})/(N_{x+1} - N_x) \quad (2)$$

To evaluate cyclic plasticity further, the ratio of minimum to maximum displacement within a loading cycle, D_{\min}/D_{\max} was analyzed. The value correlates with the amount of irreversible and reversible deformation in a single loading/unloading cycle: higher values indicate relatively more plastic (irreversible) deformation, while lower values indicate the opposite. Changes in this ratio with N indicate softening for increasing ratios and hardening for decreasing ratios.

The cyclic indents were imaged by the scanning probe microscopy (SPM) mode of the nanoindenter. The

topography images of two indents were analyzed for each material regarding size and volume of the indent and pile-up using the open-source program Gwyddion.²⁴

2.2.2 | Macrofatigue behavior

Stress-controlled stepwise load increase (LIT) tests were performed in ambient air at room temperature on an ElectroPuls E3000 (Instron, Buckinghamshire, UK). The long axis of the samples was aligned exactly with the loading axis to avoid bending stresses. Force was measured using the inbuilt 5-kN load cell (accuracy $\pm 0.005\%$ for $F \leq 50$ N and $\pm 0.5\%$ for $F > 50$ N). Strain was measured using an inductive displacement sensor (multi-NCNT Series 300, Micro-Epsilon Messtechnik, Ortenburg, Germany) with a resolution of 0.4% that was attached to the grips. Calibration was carried out for an increasing load series in the elastic regime, using 1-mm-long strain gauges with a tolerance of ± 0.85 $\mu\text{m}/\text{m}$ (FLK-1-23, Tokyo Measuring Instruments Laboratory Co., Ltd., Tokyo, Japan) mounted on the gauge length of one sample. We note that strain values are averaged over the whole measurement volume as soon as strain localization (e.g., as more localized plasticity during cyclic hardening and softening) occurs

Three samples of each composition were tested using a sinusoidal waveform with completely reversed loading ($R = \sigma_{\min}/\sigma_{\max} = -1$) at a frequency of 5 Hz. Loading started with a stress amplitude of 10 MPa; after a number of 10^4 cycles, the stress amplitude was increased by 5 MPa over 10^3 cycles. These steps were repeated until specimen failure. From the hysteresis loops, the plastic strain amplitude, plastic mean strain ($\epsilon_{m,p} = \epsilon_{m,t} - \sigma_m/E$, with $\epsilon_{m,t}$ = total mean strain, σ_m = mean stress, E = Young's modulus) and minimum and maximum strain were determined by custom-made code. In order to precisely determine the stress amplitude for which the plastic strain amplitude increases significantly, thus estimating the cyclic yield strength and from this the fatigue endurance limit,¹³ the plastic strain amplitude, plotted versus the number of cycles, was fitted by a third-degree polynomial function, and the first derivation of this curve was used to determine the change in slope. A “significant” change was defined as a deviation of the first derivation from a linear progression over the number of cycles.

Topography of the fracture surfaces was investigated using a Phenom XL (Thermo Fisher Scientific, Waltham, USA) scanning electron microscope at an accelerating voltage of 10 kV. Surface filter with shortest and longest cut-off wavelengths of $\lambda_s = 223.61$ nm and $\lambda_c = 282.84$ μm , respectively, were employed to determine the mean arithmetic height S_a .

2.3 | Texture analysis

In order to investigate the influence of texture as a function of the reinforcement content, X-ray diffraction (XRD) measurements were performed on longitudinal sections (cut parallel to ED), corresponding to the X-ray direction being orthogonal to ED, using a psi-diffractometer (Huber) with a position sensitive detector (PSD-50M, M. Braun GmbH), monochromatic Co K_{α} radiation, an accelerating voltage of 40 kV and a collimated beam diameter of 2 mm. To observe the intensity distribution of the $\{10\bar{1}0\}$, $\{0002\}$, $\{10\bar{1}1\}$, $\{10\bar{1}2\}$, and $\{11\bar{2}0\}$ reflections, the samples were tilted (psi axis) and rotated (phi axis) in 5 deg steps from 0° to 55° and 0° to 355° , respectively. The orientation distribution function

was determined from the experimental data after rotation by 90° to analyze the texture in a cross-sectional plane orthogonal to ED using the ODF program system²⁵ and the Matlab software package MTEX.²⁶

3 | RESULTS

3.1 | Cyclic nanoindentation

Figure 2 shows SPM topography images and 3D elevation profiles of cyclic indents in Mg, MM, M1S_n, and M3S_n. Indent and pile-up volumes of all samples are plotted in Figure 3. The data clearly show decreasing indentation sizes and depths for mechanically milled MM as

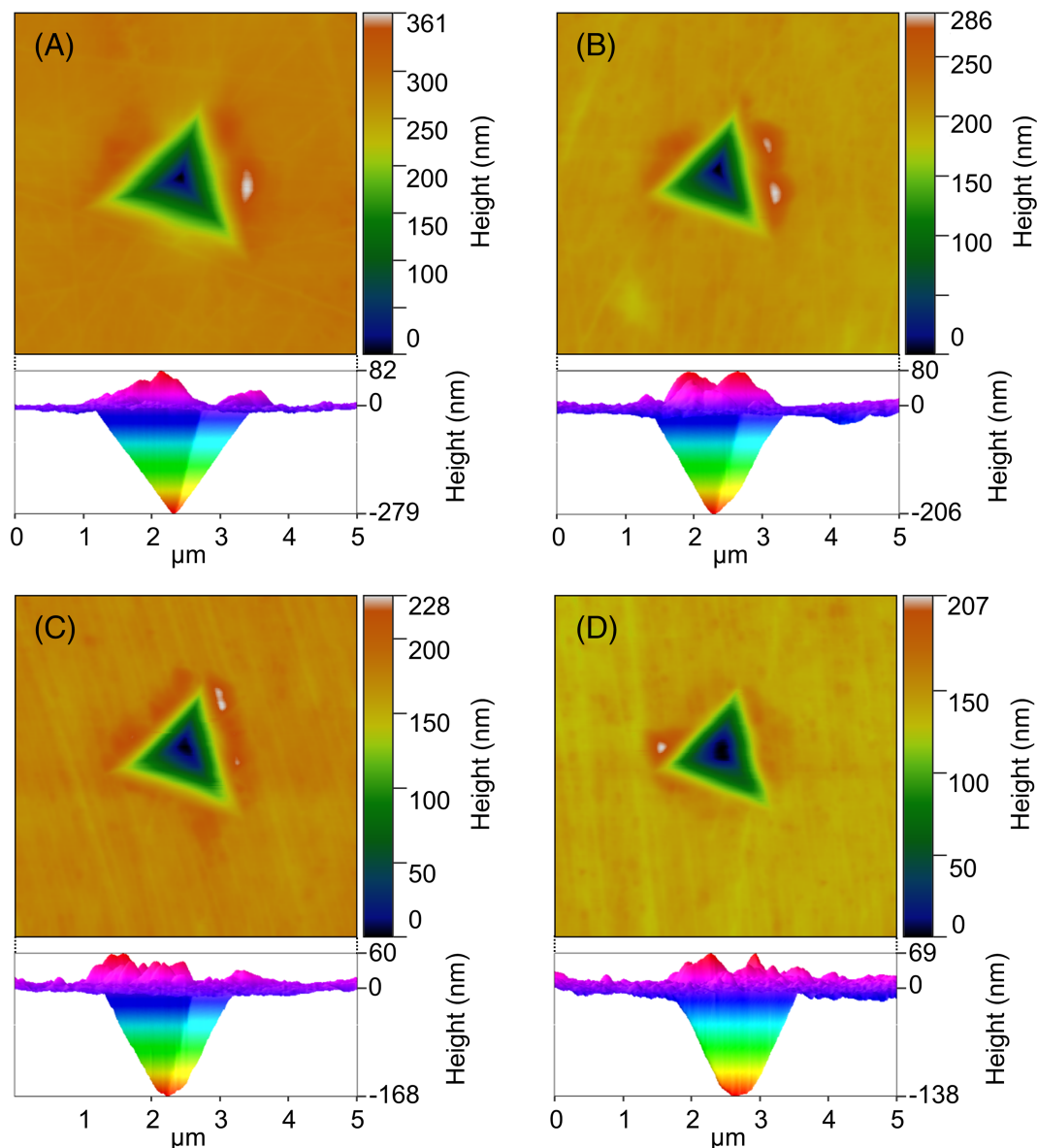


FIGURE 2 SPM topography images (top) and 3D elevation profiles (bottom) of nanoindents, loaded up to $N = 10^5$ cycles, showing pile-up in all samples: (A) Mg, (B) MM, (C) M1S_n, and (D) M3S_n [Colour figure can be viewed at wileyonlinelibrary.com]

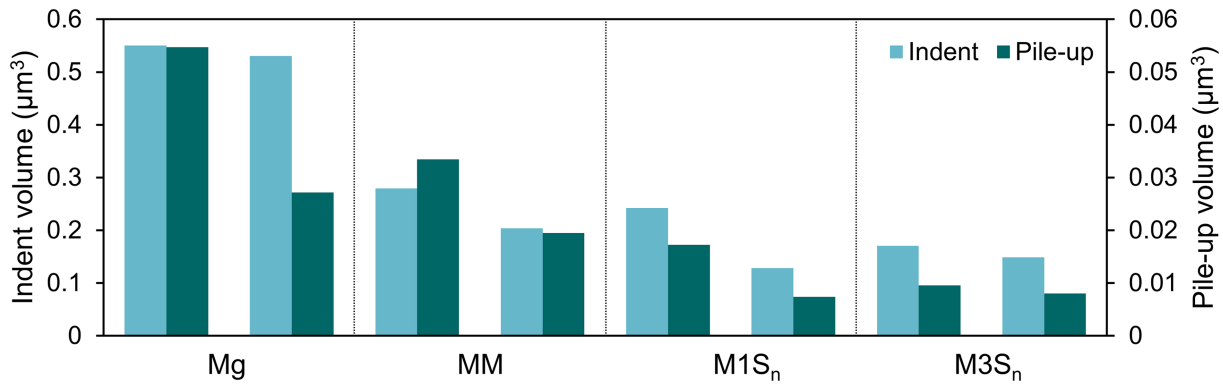


FIGURE 3 Indent and pile-up volumes after cyclic nanoindentation up to $N = 10^5$ cycles for two typical indents per material [Colour figure can be viewed at wileyonlinelibrary.com]

compared to nonmilled Mg, and with increasing reinforcement content for the mechanically milled nanocomposites. Significant pile-up is seen at the edges of all indents, but no cracks were observed in the vicinity of any of the indents.

Figure 4A shows the average ratios of D_{\min} to D_{\max} plotted versus N . All sample types exhibit a steep increase within the first ten cycles, followed by smaller increases with ongoing cyclic loading. While the Mg curve has a slightly convex shape for higher cycle numbers and a linear slope for $N \geq 10^4$, the curves of the nanocomposites have slightly concave progressions with an increasing trend for higher cycle numbers. This is most pronounced for M3S_n. Over the investigated range of cycle numbers, Mg exhibits the highest values of D_{\min}/D_{\max} . Mechanical milling and nanoparticle reinforcement lead to lower values, with similar ratios for MM and M1S_n and much lower values for M3S_n.

The average values of $\Delta D_{\min-\text{norm}}$ are plotted versus N in Figure 4B. Two regimes with significantly different behavior are observed: the “incipient” fatigue regime up to $N = 10^3$ and the “advanced” regime from $N = 10^4$ to $N = 10^5$. The incremental plastic deformation per cycle decreases over N . Within the first 10 cycles, $\Delta D_{\min-\text{norm}}$ decreases by more than 60% for all materials, and hardly any differences are observed between the different materials. Subsequently, $\Delta D_{\min-\text{norm}}$ continues to decrease, but with a lower rate, and only small changes can be identified with increasing cycle number. Up to $N = 10^4$, Mg and M3S_n exhibit the overall highest and lowest values, respectively, while the values of MM and M1S_n are very similar and lie between the Mg and M3S_n curves. The same differences between the materials are observed in the advanced regime. However, while MM exhibits a saturation state with constant values for $N \geq 2 \cdot 10^4$, the values of all other samples slightly further decrease to higher cycle numbers, after which they also enter a

saturation state. The numbers of cycles, for which saturation is reached, increase with increasing reinforcement content, up to $N = 7 \cdot 10^4$ for M3S_n. For M3S_n, a slightly increasing trend is observed for higher cycle numbers beyond this threshold.

3.2 | Estimation of the fatigue endurance limit from load increase tests

Figure 5A shows typical progressions of plastic strain amplitude ($\varepsilon_{a,p}$) versus N together with fitted polynomial functions from stress-controlled macrofatigue tests, performed with $R = -1$. The small values and the relatively high scatter of $\varepsilon_{a,p}$ make it difficult to extract the cyclic yield strength from the original curves. Fitting polynomials, and evaluating the first derivative, allows clear determination of the critical stress amplitude, where $\varepsilon_{a,p}$ becomes significant.²⁰ The first derivatives of the fits of the plastic strain amplitude versus the number of cycles highlight the change in $\varepsilon_{a,p}$ with increasing stress amplitude (Figure 5B). The range where the slope of $\varepsilon_{a,p}$ shows a significant change from the initially extremely low values indicates the estimation value of the cyclic yield strength and, thus, of the endurance limit. This range of significant change in $\varepsilon_{a,p}$ is marked with arrows. From these graphs, we estimate an endurance limit for MM of about 95 MPa. Both nanocomposites, M1S_n (data not shown) and M3S_n, exhibit a higher value of about 110 MPa. The value for Mg is much lower than for the mechanically milled materials (60 MPa; data not shown).

3.3 | Cyclic deformation behavior

Figure 6A shows the development of $\varepsilon_{a,p}$, averaged over each loading step, versus N and versus σ_a for the

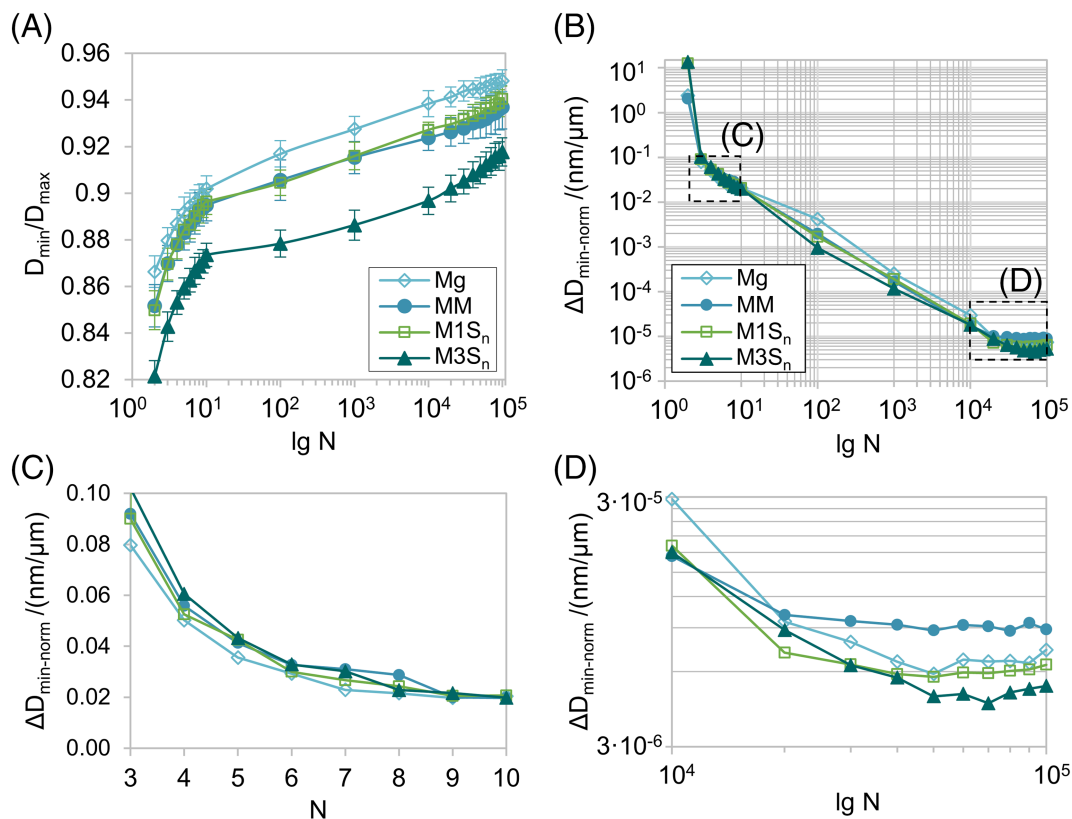


FIGURE 4 Cyclic deformation behavior during nanofatigue loading: (A) average values and standard deviations of D_{min}/D_{max} plotted versus N ; (B–D) average $\Delta D_{min-norm}/N$ -curves (B) for the whole test, (C) in the “incipient” regime ($N \leq 10^3$ cycles), (D) in the “advanced” regime ($N \geq 10^4$ cycles). The regions shown in panels (C) and (D) are marked with dotted rectangles in (B). For standard deviations see supplementary figure S1 [Colour figure can be viewed at wileyonlinelibrary.com]

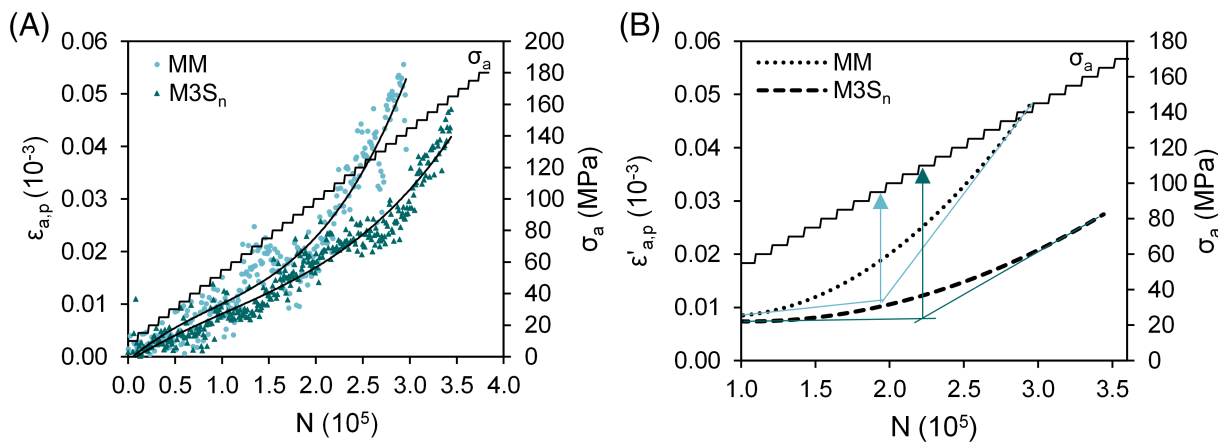


FIGURE 5 Progression of plastic strain amplitude versus number of cycles of mechanically milled Mg (MM) and Mg–SiC nanocomposites M3S_n in LIT: (A) typical examples of $\epsilon_{a,p}/N$ -curves (dotted graphs) together with their fitted polynomial functions (full lines); (B) plots of the differentiated fit functions for $\epsilon_{a,p}$ with the estimated fatigue endurance limits, marked by arrows [Colour figure can be viewed at wileyonlinelibrary.com]

same specimens as shown in Figure 5. Averaging over the loading steps highlights some typical aspects of the cyclic deformation behavior. In the beginning, all materials exhibit a linear increase in $\epsilon_{a,p}$ with

increasing stress amplitude. In the further course, Mg shows two steep increases between 40 and 45 MPa as well as 60 and 90 MPa resulting in the highest overall $\epsilon_{a,p}$ values.

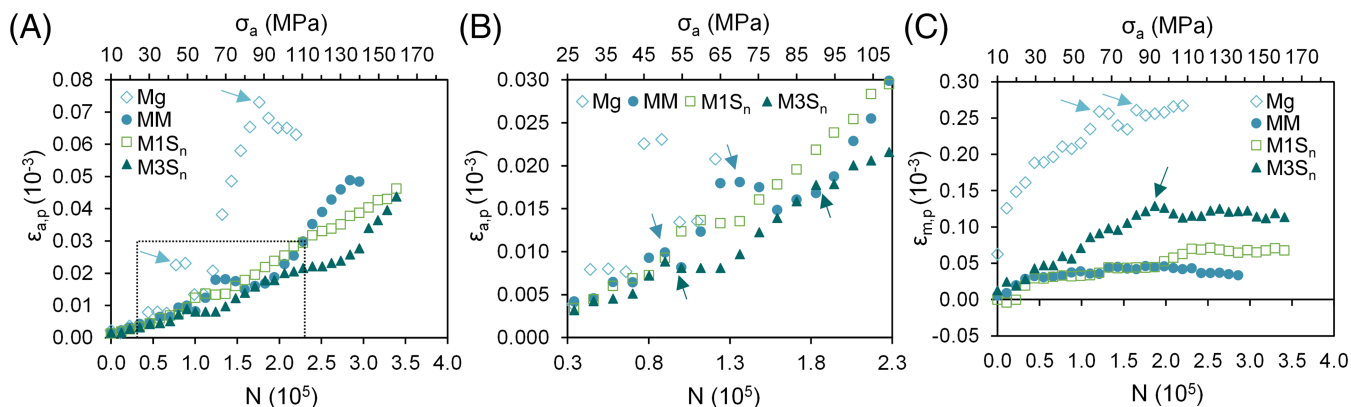


FIGURE 6 Cyclic deformation and cyclic creep behavior of Mg, MM, M1S_n and M3S_n averaged over each load step: (A) plastic strain amplitude ($\epsilon_{a,p}$), (B) magnified view of the progression of $\epsilon_{a,p}$ in the lower loading regime (marked by the dotted rectangle in panel A), and (C) plastic mean strain ($\epsilon_{m,p}$) plotted versus number of cycles (N) and stress amplitude (σ_a) [Colour figure can be viewed at wileyonlinelibrary.com]

To better discriminate differences between the mechanically milled materials, a magnified view of the lower loading regime (dotted rectangle in Figure 6A) is shown in Figure 6B. These materials, MM, M1S_n, and M3S_n, exhibit similar values of the plastic strain amplitude up to a stress amplitude of 50 MPa. MM shows two significant cyclic hardening events (blue arrows in Figure 6B) between 50 and 55 MPa as well as 75 and 80 MPa each followed by strong cyclic softening. After the second cyclic hardening event, the plastic strain amplitude for MM steadily increases until it reaches a saturation state at 135 MPa shortly before fracture in the next loading step (140 MPa). Overall, M1S_n shows cyclic hardening with only two small plateau regions, between 60 and 65 MPa and at 150 MPa right before fracture at 160 MPa. M3S_n exhibits only one plateau between 55 and 65 MPa. In the further course, $\epsilon_{a,p}$ shows slight cyclic hardening at 90 MPa and 115 MPa. From 140 MPa onwards, $\epsilon_{a,p}$ of M3S_n almost linearly increases until fracture at 160 MPa.

Figure 6C shows the development of plastic mean strain over the number of cycles and corresponding stress amplitude. Mg exhibits pronounced creep in the positive direction. In some loading steps, namely, 55 to 65 MPa and 80 MPa, $\epsilon_{m,p}$ shows a more pronounced increase, followed by a decrease over several loading steps. From 90 MPa onwards, only a small further increase in $\epsilon_{m,p}$ is observed. The decrease in $\epsilon_{m,p}$ correlates with the cyclic hardening phases described above (Figure 6A). MM and M1S_n exhibit almost similar $\epsilon_{m,p}$ values up to a stress amplitude of 95 MPa, and much lower than those observed for Mg. In the further course, $\epsilon_{m,p}$ decreases slightly for MM, while $\epsilon_{m,p}$ of M1S_n increases up to a stress amplitude of 115 MPa and only remains constant

until fracture for higher stress amplitudes. M3S_n increases up to a stress amplitude of 95 MPa showing significantly more pronounced tensile creep than both, MM and M1S_n. From 95 MPa onwards, $\epsilon_{m,p}$ first slightly decreases until 110 MPa and then remains more or less constant until fracture.

3.4 | Fracture surface morphology

Figure 7 shows roughness profiles, plotted as color maps, of the fracture surfaces near the fatigue origin (left) and far from the fatigue origin (right) of MM (A,D), M1S_n (B,E), and M3S_n (C,F). Fatigue failure generally started on the surface, at one of the edges of the rectangular samples. Dark red color is associated with peaks, whereas blue color indicates valleys. The mean arithmetic height S_a is denoted in each image. As to be expected, all materials show lower roughness near the fatigue origin than further away from it. MM and M1S_n exhibit very similar roughness values, both at the fatigue origin and further away from it. In contrast, M3S_n has a very smooth fracture surface near the fatigue origin but a relatively rough surface further away. With a value of 1.90 μm near the fatigue origin and 8.63 μm further away, S_a only reaches a little bit more than half (60%) the values measured for MM and M1S_n near the fatigue origin, but double the values of MM and M1S_n further away.

3.5 | Textures

Pole figures of Mg, MM, M1S_n, and M3S_n, illustrating the density distribution of crystallographic grain orientations

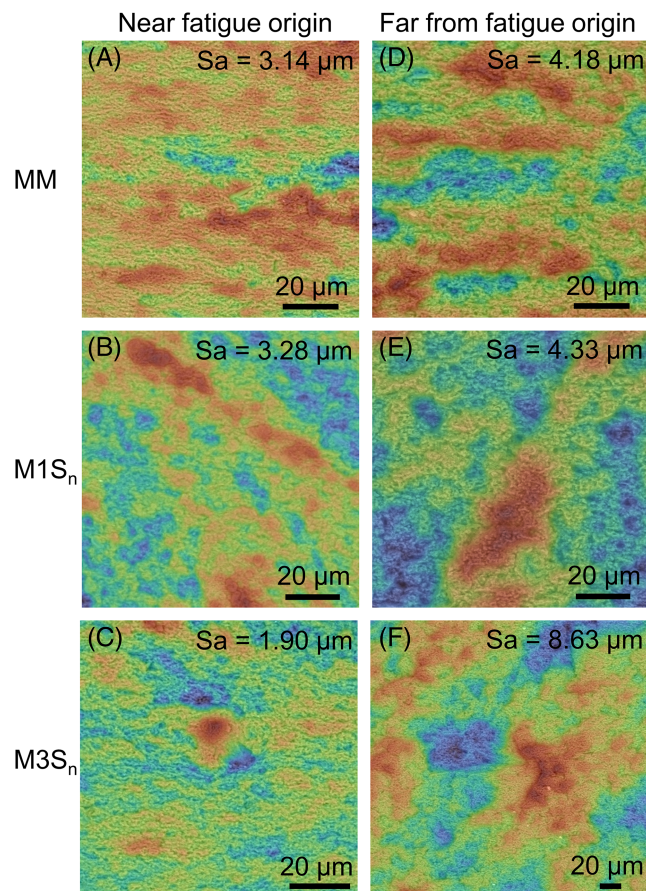


FIGURE 7 Roughness profiles as color maps near the fatigue origin (A–C) and far from the fatigue origin (D–F) of (A,D) MM, (B,E) M1S_n, and (C,F) M3S_n. Dark red indicates peaks whereas blue indicates valleys. The mean arithmetic height S_a is denoted in each profile [Colour figure can be viewed at wileyonlinelibrary.com]

in the basal (0001), prismatic ($10\bar{1}0$), and pyramidal planes ($10\bar{1}1$), are represented in Figure 8. As to be expected, Mg shows a strong texture. The two maxima of the (0001) plane indicate that the basal planes are parallel to ED (Figure 8A). The three maxima of the ($10\bar{1}0$) pole figure correspond to a preferential orientation of the prism planes of the hexagonal unit cell. Mechanical milling of the powders leads to a much weaker texture, both for the non-reinforced MM and the nanocomposites (Figure 8B–D). Specifically, we observe weakening of the texture by rotation of the basal plane from its parallel orientation to the ED. The (0001) pole figure of the nanocomposites (Figure 8C,D) shows two maxima, whereby the intensity is slightly higher in M3S_n. All samples also exhibit a strong maximum in the ($10\bar{1}0$) pole figure, which is associated with the fiber texture. Here, too, the intensity increases in M3S_n compared to M1S_n.

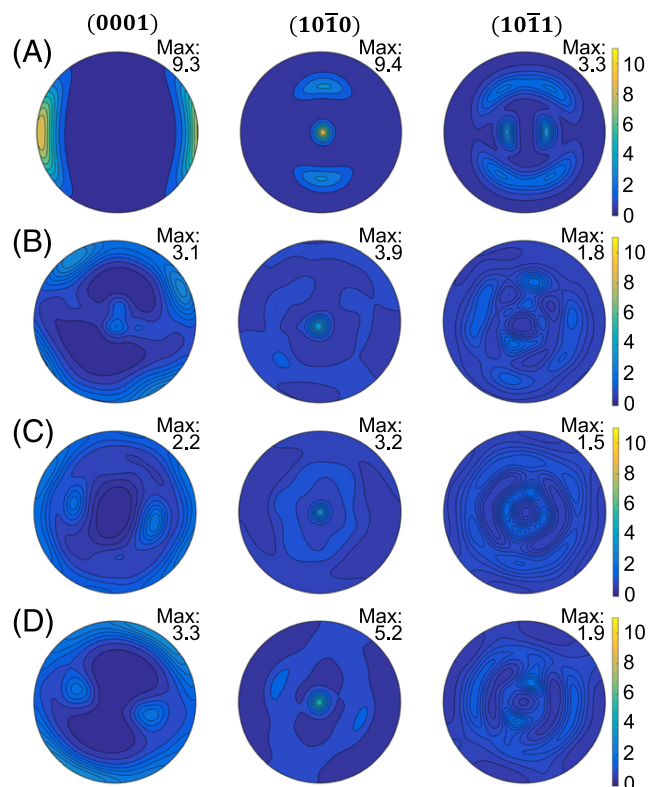


FIGURE 8 Pole figures of (A) Mg, (B) MM, (C) M1S_n, and (D) M3S_n illustrating the density distribution of crystallographic grain orientations in cross-sections (note: ED is orthogonal to the viewing plane) for the basal (0001), prismatic ($10\bar{1}0$), and pyramidal planes ($10\bar{1}1$) [Colour figure can be viewed at wileyonlinelibrary.com]

4 | DISCUSSION

Cyclic fatigue behavior is one of the most important properties to be considered when designing parts in motion. The deformation behavior under fatigue loading is influenced by the manufacturing processes and the resulting microstructure. Here, we investigated the cyclic deformation behavior of Mg–SiC nanocomposites on the nanoscale using cyclic nanoindentation and on the macroscale using stress-controlled LIT. Due to the small number of samples available, LIT was a helpful method to estimate the fatigue endurance limit and to gain insights into the cyclic deformation behavior. Interestingly, cyclic nanoindentation and macroscopic, fully reversed cyclic loading lead to similar observations despite the different loading conditions. Grain size, defect density, and texture strongly determine the fatigue limit and the cyclic deformation capability by complex interactions.

We propose that the interaction of different microstructural features and the corresponding strengthening

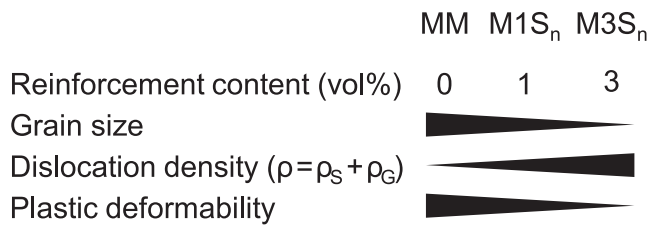


FIGURE 9 Microstructural features and plastic deformability dependent on the reinforcement content. Dislocation density ρ comprises density of statistically stored dislocations (ρ_S) and of geometrically necessary dislocations (ρ_G). ρ_G increases with increasing amount of grain boundaries and reinforcement content

mechanisms, including grain boundary strengthening, work hardening, and precipitation hardening, together with crack–particle interactions contribute to different extents to cyclic plastic deformability, leading to different fatigue failure mechanisms in the different materials. Figure 9 summarizes the influence of reinforcement content on microstructural features, that is grain size and dislocation density, and on plastic deformability. In the following, we will discuss these connections in detail.

4.1 | Specifics of the microstructure

The deformation behavior under fatigue loading is influenced by the manufacturing processes and the resulting microstructural parameters. We previously showed that mechanical milling leads to nanocrystalline and nanocomposite powders.^{22,23} Even during the following processing steps, comprising cold-isostatic pressing, sintering, and hot extrusion, nanocrystallinity is preserved. Another important microstructural factor influencing the deformation behavior is texture. Mg wrought alloys usually develop a pronounced basal fiber texture during extrusion.^{27,28} In contrast, we unexpectedly observed a weak, tilted basal fiber texture in the mechanically milled materials. The weak texture and the tilting of the c-axis can only be partially explained by the decrease in grain size and the randomization of grain orientations due to dynamic recrystallization.^{17,29} A further possible explanation is a slight torsional stress exerted during extrusion due to the shape of the die. A similar effect of a spiral-shaped basal texture, where the c-axis deviates outwards instead of being oriented orthogonal to the extrusion direction, was described by She et al. for on-line twist extrusion.³⁰

Further, the extruded nanocomposites contain a higher amount of dislocations as compared to the non-reinforced but mechanically milled pure magnesium variant MM.^{22,31} This is caused by extensive plastic

deformation during mechanical milling, leading to a higher dislocation density in the nanoparticle reinforced variants. Defect density is further influenced by the difference in thermal expansion coefficients between SiC particles and Mg matrix. All this results in a build-up of defects around the nanoparticles during the manufacturing process and thus in an increase in defect density in the nanocomposites. Although the higher dislocation density that is reached due to the nanoparticles triggers dynamic recrystallization which explains the small retained grain size, not all defects are removed during the process. This observation is in good agreement with results reported by Koneva et al.,³² where strong barriers such as nanoparticles and grain boundaries lead to the accumulation of geometrically necessary dislocations (ρ_G). These retained dislocations significantly influence the mechanical behavior of the nanocomposites by determining the plastic deformability. Grain size decreases and defect density increases with increasing reinforcement content because interactions between (a lower volume fraction of) nanoparticles and dislocations lead to less plastic deformation and less dynamic recrystallization during extrusion in M1S_n as compared to M3S_n.²² As a result, M1S_n also has a lower quasistatic strength but a higher ductility than M3S_n and microhardness increases as a function of the decrease in grain size and increase in dislocation density.²²

4.2 | Microstructural effects on fatigue endurance

Pure Mg showed a fatigue endurance limit of 60 MPa, estimated from macro-LIT. This value is comparable with those commonly reported for pure magnesium.²⁰ As expected, the estimation values increased by using mechanically milled powders and, further, by addition of nanoparticles. Since the main microstructural difference between Mg and MM is the grain refinement of the latter, the higher endurance limit of MM compared to Mg is therefore likely due to Hall–Petch hardening by grain refinement. Increasing nanoparticle contents in the nanocomposites lead to even smaller grain sizes²² and a decrease in tension-compression-asymmetry, which explains the increase in endurance limit when nanoparticles are added. Compared to Mg, the materials made from mechanically milled powders, namely, MM, M1S_n, and M3S_n, show a higher plastic deformability due to their extremely small grain size. Concomitantly, grain boundary strengthening triggers the activation of non-basal slip. This finding highlights the very positive effect of mechanical milling as a first process step. Surprisingly, however, increasing reinforcement contents had no

additional positive effect, despite the decrease in grain size, and the corresponding higher work hardening capability and quasistatic strength. An explanation is the increased dislocation density with increasing reinforcement content due to the pinning-effect of the nanoparticles, which decreases plastic deformability and facilitates faster crack growth once a fatigue crack has been initiated. Relatively lower energy absorption and faster crack velocities near the fatigue origin, suggesting a more brittle fracture behavior for small crack lengths, as compared to MM and M1S_n, are supported by the observation of a very smooth fracture surface of M3S_n near the fatigue origin. Similarly, Sattari and Atrian³³ describe a reduced dimple size, that is a more brittle fracture mode, with increasing SiC content in fatigued Al–SiC nanocomposites. Further explanation of the very smooth fracture surface near the fatigue origin in M3S_n is given by the geometric model for roughness-induced crack closure.³⁴ The authors stated that the extent of crack closure is a strong function of surface roughness, mode II crack tip displacement, and grain size. The model suggests that the plastic zone size exceeds the grain size during fatigue initiation, especially in case of M3S_n with the smallest grain size of all investigated materials. This leads to a more planar crack path due to activation of more than one slip system.

The effect of increasing brittleness with increasing nanoparticle content is counteracted by a higher propensity to crack deflection and energy absorption due to microcrack formation at particle–matrix interfaces. We see this in regions far from the fatigue origin, where crack deflection leads to a plastic zone that is smaller than the grain size. Consequently, we measure the highest roughness on the fracture surfaces in M3S_n, together with a serrated fracture path due to slip along one single slip system.

We therefore conclude that the resistance against crack formation and against crack growth both play important but different roles for the deformation behavior of M1S_n and M3S_n thus explaining the similar fatigue endurance limits.

4.3 | Macroscale cyclic deformation behavior

We further evaluated stress-controlled LIT regarding deformation and creep behavior. Our observation of tensile cyclic creep is in good agreement with our quasistatic results where we observed higher compressive than tensile strength.^{35,36} This is surprising in light of the other reports on extruded magnesium materials. Generally, a strong ring-fiber texture is observed which leads to lower

strength in compression as compared to tension.^{37,38} This asymmetric deformation behavior, the so-called strength difference effect (SDE), is due to inhibition of basal slip and activation of twinning under compression.^{39,40} Reasons for the low and inverse tension-compression asymmetric behavior that we see in our mechanically milled Mg–SiC nanocomposites may be:

- i) weakening of the texture due to an increase in dynamic recrystallization with increasing reinforcement content,
- ii) the slightly tilted texture, since the tension-compression yield asymmetry is orientation-dependent,³⁸ and
- iii) the low total strain amplitudes of less than 0.2% resulting in an overall decreased asymmetry.⁴⁰

Texture strongly influences the activation of certain slip systems and/or twinning. A weak texture involves a significant number of randomly oriented grains that exhibit a lower Schmid factor for extension twinning. Thus, activation of twinning is hindered, leading to more pronounced work hardening. Hassan and Lewandowski⁸ ascribed the work hardening to a higher density of pre-existing dislocations, dislocation–dislocation interaction, and interactions of mobile dislocations with nanoparticles leading to forest dislocations. The small grain sizes (<1 μm) and the tilted, weak fiber texture suggest that negligible or no twinning took place⁴¹ and that consequently, secondary deformation modes such as non-basal dislocation slip, are more prominent.⁴² This conjecture is confirmed by the observation of Lin et al.,⁴³ who reported for equal channel angular extrusion of an AZ31 alloy easier slip in tensile testing than in compression testing, resulting in lower yield strength and ultimate tensile strength, due to the preferred orientation of the basal planes.

Maxima in the pole figures can be associated with the activity of different slip systems. Based on observations by Minárik et al.⁴⁴ on the influence of texture in the Mg alloy LAE442 on the deformation mechanisms we deduce that prismatic slip, associated with maxima in the (0001) pole figure and additional texture intensities in the (10 $\bar{1}$ 0) pole figure, is the predominant deformation mechanism in our Mg material. Accordingly, basal slip predominates in the nanocomposites, as it is associated with maxima in the (0001) pole figures. We therefore assume that activation of prismatic slip in the nanocomposites can be a reason for the significantly higher endurance limit compared to pure Mg.

Comparison of $\epsilon_{m,p}$ of Mg with MM, M1S_n, and M3S_n indicates reduced cyclic creep for the latter

(see Figure 6C). These observations well match the findings of Dieringa,⁴⁵ who reported improved creep resistance in mechanically milled composites. A reason for higher cyclic creep under tension of M3S_n compared to MM and M1S_n may be hindered twinning due to a small grain size and the pinning-effect of the nanoparticles resulting in faster crack initiation.

We further conclude that the relatively high plastic deformation indicated by a steep increase in $\epsilon_{a,p}$ over several loading steps of M3S_n (Figure 6A) is due to microcrack formation and growth and less to real plastic deformation.¹⁷ This conclusion is corroborated by the observation of decreasing slopes of the hysteresis loops, with cyclic loading (Figure S2).

4.4 | Nanoscale cyclic deformation behavior

High cycle fatigue tests on the nanoscale, performed by cyclic nanoindentation, are still very scarce. For the first time, we characterized the nanofatigue behavior of Mg–SiC nanocomposites by repeatedly nanoindenting the same position up to 10⁵ cycles. The load-indentation curves yield information on the cyclic deformation behavior, and quantitative evaluation of indent and pile-up volumes reflects the plastic deformation capability of the different nanocomposites.

As to be expected, the largest indents and the highest pile-up were observed for Mg. This is associated with its relatively low strength and its low potential for work hardening.⁴⁶ The latter allows relatively high amounts of plastic deformation and easy propagation of the plastic zone. Conversely, in the case of nanoparticle reinforced composites, the regions of higher defect density surrounding the nanoparticles, and the extremely small grain size of the nanocomposites hinder dislocation movement and thus hamper the propagation of the plastic zone developing beneath the indenter tip. This leads to less plastic deformation and, concurrently, to smaller indent and pile-up sizes with increasing reinforcement contents.

The significant change in D_{\min}/D_{\max} over the course of loading hints to significant plastic deformation and cyclic hardening in all materials. Interestingly, we see only little local variation in the behavior between indents performed at different positions in one material, in contrast to what we observed for an Al–Si–Mg alloy.¹² This is due to the much finer, homogeneous microstructure of the materials investigated here. Thus, the nanoindents are much larger than the typical microstructural unit, and we probe volumes of interest that represent the bulk

material. In materials with a coarser microstructure, the nanocyclic deformation behavior varies to a great extent depending on indent position. This applies when the mean distance between particles or precipitates in the volume beneath the indent is relatively large as compared to indent size or when grain size is so large that single grains are indented and differences in grain orientation become crucial for plastic deformation (e.g., Schmahl et al.¹² and Bočan et al.⁴⁷).

MM showed a steeper incline in D_{\min}/D_{\max} in the advanced regime compared to Mg. This can be related to a higher degree of work hardening, due to the smaller grain size and higher defect density. These two parameters lead to an internal reaction stress that lowers the energy gap to the critical resolved shear stress (CRSS). Thus, in the case of MM, nonbasal slip is activated more easily. Compared to the other compositions, M3S_n exhibits the smallest grain size and highest defect density. It further shows the least plastic deformation with increasing number of cycles, which is mainly attributed to the greater restriction of plastic flow by the higher content of nanoparticles and the resulting smaller distances between them.

This observation is also reflected in the progressions of $\Delta D_{\min-\text{norm}}$ with the number of cycles: MM shows the highest incremental plastic deformation. Surprisingly, Mg and M1S_n exhibit very similar curves with almost the same plastic deformation range. Possible reasons are the low number of independent slip systems in the case of Mg and the nanoparticle-dislocation interaction in the case of M1S_n. As compared to M1S_n, the higher nanoparticle content in M3S_n leads to a significant decrease in $\Delta D_{\min-\text{norm}}$ with increasing numbers of cycles. In the late advanced regime, however, the incremental plastic deformation of M3S_n increases, which may possibly be explained by the activation of nonbasal slip.

4.5 | Comparison of nanofatigue and macrofatigue behavior

MM, M1S_n, and M3S_n show similar plastic deformation behavior in both nanofatigue and macrofatigue tests up to 2·10⁴ and 10⁵ cycles, respectively. Surprisingly, Mg exhibited lower $\epsilon_{a,p}$ values than MM in the nanofatigue tests but higher values in the macrofatigue tests. We attribute this observation to the absence of microcrack formation in the nanofatigue tests. Similar to the macrofatigue tests, we hypothesize that the main plastic deformation mechanism in cyclic nanoindentation is dislocation sliding and that no or only minimal twinning is induced.

5 | CONCLUSIONS

This study contributes in several ways to our understanding of the cyclic fatigue behavior of Mg–SiC nanocomposites on both the nanoscale and macroscale. Macrofatigue tests showed that mechanical milling of the powders leads to a tremendous increase in the fatigue endurance limit. This is due to the higher amount of grain boundaries restricting dislocation movements. Dislocation movements are additionally hindered by nanoparticles in the nanocomposites. The results further indicate that the plastic deformation behavior determined through cyclic nanoindentation tests is comparable to the behavior observed in macrofatigue tests. Thus, using cyclic nanoindentation allows fast and easy assessment of material performance with a small number of samples and with minimal material consumption, thus saving time and cost intensive macrofatigue tests.

We conclude that nanofatigue tests directly predict the plastic deformation behavior on the macroscale if the interaction volume below the cyclic nanoindent is representative for the bulk microstructure.

ACKNOWLEDGMENTS

The authors gratefully acknowledge the financial support by the DFG (Deutsche Forschungsgemeinschaft), and we are grateful to Fraunhofer Institute for Ceramic Technologies and Systems (IKTS, Dresden) for performing the hot isostatic pressing. The authors thank Rigerta Tola for sample preparation, Reinhard Meinke for support with macrofatigue testing, and Merle Schmahl for assistance during cyclic nanoindentation testing. The authors further thank Sören Müller and René Nitschke, Extrusion Research and Development Center (FZS), Metallic Materials, TU Berlin for execution and support during hot extrusion, and Jonas Schmidt, Metallic Materials, TU Berlin for the texture measurements. Thanks go to Fraunhofer Institute for Production Systems and Design Technology (IPK) for cutting the fatigue specimens using EDM. We are further grateful to Christoph Fahrenson, Central Electron Microscopy Unit (ZELMI), TU Berlin, for his support during SEM analyses. Open Access funding is provided by Projekt DEAL.

CONFLICT OF INTEREST

The authors declare that there is no conflict of interest.

AUTHOR CONTRIBUTIONS

D. Hübler: Conceptualization (supporting), Formal analysis, Investigation, Validation, Visualization, Writing – Original Draft Preparation, Writing – Review & Editing; **K. Winkler:** Software, Data curation, Validation, Writing – Review & Editing; **R. Riedel:** Resources, Writing –

Review & Editing; **S. Kamrani:** Conceptualization (lead), Project Administration, Funding acquisition, Writing – Review & Editing; **C. Fleck:** Conceptualization (supporting), Methodology, Resources, Supervision, Writing – Review & Editing.

DATA AVAILABILITY STATEMENT

Data are available upon request from the authors.

ORCID

Daniela Hübler  <https://orcid.org/0000-0002-0272-9343>

REFERENCES

- Potzies C, Kainer KU. Fatigue of magnesium alloys. *Adv Eng Mater.* 2004;6(5):281-289.
- Luk MJ, Mirza FA, Chen DL, Ni DR, Xiao BL, Ma ZY. Low cycle fatigue of SiCp reinforced AA2009 composites. *Mater des (1980–2015).* 2015;66:274-283.
- Goh CS, Gupta M, Wei J, Lee LC. The cyclic deformation behavior of Mg–Y₂O₃ nanocomposites. *J Compos Mater.* 2008; 42(19):2039-2050.
- Chamos AN, Charitidis CA, Skarmoutsou A, Pantelakis SG. An investigation on the high stress sensitivity of fatigue life of rolled AZ31 magnesium alloy under constant amplitude fatigue loading. *Fatigue Fract Eng Mater Struct.* 2010;33(4): 252-265.
- Luo A. Processing, microstructure, and mechanical behavior of cast magnesium metal matrix composites. *Metall Mater Trans a.* 1995;26(9):2445-2455.
- Lan J, Yang Y, Li X. Microstructure and microhardness of SiC nanoparticles reinforced magnesium composites fabricated by ultrasonic method. *Mater Sci Eng A.* 2004;386(1–2):284-290.
- Zhang Z, Chen DL. Contribution of Orowan strengthening effect in particulate-reinforced metal matrix nanocomposites. *Mater Sci Eng A.* 2008;483–484:148-152.
- Hassan HA, Lewandowski JJ. Effects of particulate volume fraction on cyclic stress response and fatigue life of AZ91D magnesium alloy metal matrix composites. *Mater Sci Eng A.* 2014;600:188-194.
- Koike J, Kobayashi T, Mukai T, et al. The activity of non-basal slip systems and dynamic recovery at room temperature in fine-grained AZ31B magnesium alloys. *Acta Mater.* 2003;51(7): 2055-2065.
- Gall K, Biallas G, Maier HJ, et al. In-situ observations of high cycle fatigue mechanisms in cast AM60B magnesium in vacuum and water vapor environments. *Int J Fatigue.* 2004;26(1): 59-70.
- Jain S, Gokhale A, Jain J, Singh SS, Hariharan K. Fatigue behavior of aged and solution treated AZ61 Mg alloy at small length scale using nanoindentation. *Int Symp Phys Mater.* 2017; 684:652-659.
- Schmahl M, Märten A, Zaslansky P, Fleck C. Nanofatigue behaviour of single struts of cast A356.0 foam: cyclic deformation, nanoindent characteristics and sub-surface microstructure. *Mater des.* 2020;195:109016.
- Srivatsan TS, Al-Hajri M, Lam PC. The quasi-static, cyclic fatigue and final fracture behavior of a magnesium alloy metal-matrix composite. *Compos B Eng.* 2005;36(3):209-222.

14. Vaidya AR, Lewandowski JJ. Effects of SiCp size and volume fraction on the high cycle fatigue behavior of AZ91D magnesium alloy composites. *Mater Sci Eng a*. 1996;220(1-2): 85-92.
15. Jabbari AH, Delavar H, Sedighi M. High cycle fatigue behavior of magnesium matrix nanocomposite at elevated temperatures. *Mech Mater*. 2020;142:103278.
16. Jabbari AH, Shafiee Sabet A, Sedighi M, Jahed H, Sommitsch C. Low cycle fatigue behavior of magnesium matrix nanocomposite at ambient and elevated temperatures. *Mater Sci Eng a*. 2020;793:139890.
17. Tekumalla S, Bibhanshu N, Shabadi R, Suwas S, Ha TMH, Gupta M. Evolution of texture and asymmetry and its impact on the fatigue behaviour of an in-situ magnesium nanocomposite. *Mater Sci Eng a*. 2018;727:61-69.
18. Srivatsan TS, Godbole C, Quick T, Paramsothy M, Gupta M. Mechanical behavior of a magnesium alloy nanocomposite under conditions of static tension and dynamic fatigue. *J Mater Eng Perform*. 2013;22(2):439-453.
19. Srivatsan TS, Godbole C, Paramsothy M, Gupta M. The role of aluminum oxide particulate reinforcements on cyclic fatigue and final fracture behavior of a novel magnesium alloy. *Mater Sci Eng a*. 2009;532:196-211.
20. Wolf B, Fleck C, Eifler D. Characterization of the fatigue behaviour of the magnesium alloy AZ91D by means of mechanical hysteresis and temperature measurements. *Int J Fatigue*. 2004;26(12):1357-1363.
21. Fleck C, Löhde D. Cyclic deformation behavior of newly developed microalloyed Mg wrought alloys in corrosive environment. In: Beals RS, Luo AA, Neelameggham NR, Pekkuguleryuz MO, eds. *Magnesium Technology 2007*; 2007: 275-279.
22. Penther D, Ghasemi A, Riedel R, Fleck C, Kamrani S. Effect of SiC nanoparticles on manufacturing process, microstructure and hardness of Mg-SiC nanocomposites produced by mechanical milling and hot extrusion. *Mater Sci Eng a*. 2018;738: 264-272.
23. Kamrani S, Penther D, Ghasemi A, Riedel R, Fleck C. Microstructural characterization of Mg-SiC nanocomposite synthesized by high energy ball milling. *Adv Powder Technol*. 2018;29(7):1742-1748.
24. Nečas D, Klapetek P. Gwyddion: an open-source software for SPM data analysis. *Open Physics*. 2012;10(1):181-188. <https://doi.org/10.2478/s11534-011-0096-2>
25. Bunge HJ (Ed). *Program System ODF-Analysis for Cubic Crystal Symmetry, Orthorhombic Sample Symmetry*. 2nd ed. Göttingen: Cuvillier; 1999.
26. Bachmann F, Hielscher R, Schaeben H. Texture analysis with MTEX—free and open source software toolbox. *Solid State Phenom*. 2010;160:63-68.
27. Pahlevanpour AH, Behraves SB, Adibnazari S, Jahed H. Characterization of anisotropic behaviour of ZK60 extrusion under stress-control condition and notes on fatigue modeling. *Int J Fatigue*. 2019;127:101-109.
28. Lou XY, Li M, Boger RK, Agnew SR, Wagoner RH. Hardening evolution of AZ31B Mg sheet. *Int J Plast*. 2007;23(1):44-86.
29. Kavyani M, Ebrahimi GR, Sanjari M, Haghshenas M. Texture evaluation in warm deformation of an extruded Mg-6Al-3Zn alloy. *J Magnes Alloy*. 2016;4(2):89-98.
30. She J, Peng P, Tang AT, et al. Novel on-line twist extrusion process for bulk magnesium alloys. *Mater des*. 2019;182:108011.
31. Penther D, Fleck C, Ghasemi A, Riedel R, Kamrani S. Development and characterization of Mg-SiC nanocomposite powders synthesized by mechanical milling. *Key Eng Mater*. 2017;742: 165-172.
32. Koneva N, Popova N, Fedorisheva M, Kozlov E. Geometrically necessary dislocations in deformed martensitic steel. *Adv Mater Res*. 2014;1013:23-30.
33. Sattari S, Atrian A. Investigation of deep rolling effects on the fatigue life of Al-SiC nanocomposite. *Mater Res Express*. 2018; 5(1):15052.
34. Suresh S, Ritchie RO. A geometric model for fatigue crack closure induced by fracture surface roughness. *Metall Mater Trans a*. 1982;13(9):1627-1631.
35. Hübler D. From mechanically milled powders to Mg-SiC nanocomposites: relationships between processing, microstructure and mechanical properties. *Doctoral dissertation*. Technische Universität Berlin; 2021 (yet unpublished).
36. Kamrani S, Hübler D, Ghasemi A, Fleck C. Enhanced strength and ductility in magnesium matrix composites reinforced by a high volume fraction of nano- and submicron-sized SiC particles produced by mechanical milling and hot extrusion. *Materials*. 2019;12(20):3445.
37. Yu M-H, Ma G-W, Qiang H-F, Zhang Y-Q. *Generalized Plasticity*. Berlin, Heidelberg: Springer-Verlag Berlin Heidelberg; 2006.
38. Yin DL, Wang JT, Liu JQ, Zhao X. On tension-compression yield asymmetry in an extruded Mg-3Al-1Zn alloy. *J Alloys Compd*. 2009;478(1):789-795.
39. Garcés G, Pérez P, Adeva P. Effect of the extrusion texture on the mechanical behaviour of Mg-SiCp composites. *Scripta Mater*. 2005;52(7):615-619.
40. Begum S, Chen D, Xu S, Luo A. Low cycle fatigue properties of an extruded AZ31 magnesium alloy. *Int J Fatigue*. 2009;31(4): 726-735.
41. Kaya AA. Physical metallurgy of magnesium. In: Pekkuguleryuz MO, Kainer KU, Arslan Kaya A, eds. *Fundamentals of Magnesium Alloy Metallurgy*. Woodhead Publishing Series in Metals and Surface Engineering. Woodhead Publishing; 2013:33-84.
42. Agnew SR, Yoo MH, Tomé CN. Application of texture simulation to understanding mechanical behavior of Mg and solid solution alloys containing Li or Y. *Acta Mater*. 2001;49(20): 4277-4289.
43. Lin HK, Huang JC, Langdon TG. Relationship between texture and low temperature superplasticity in an extruded AZ31 Mg alloy processed by ECAP. *Mater Sci Eng a*. 402(1-2): 250-257.
44. Minárik P, Král R, Čížek J, Chmelík F. Effect of different c/a ratio on the microstructure and mechanical properties in magnesium alloys processed by ECAP. *Acta Mater*. 2016;107: 83-95.
45. Dieringa H. Properties of magnesium alloys reinforced with nanoparticles and carbon nanotubes: a review. *J Mater Sci*. 2011;46(2):289-306.
46. Broitman E. Indentation hardness measurements at macro-, micro-, and nanoscale: a critical overview. *Tribol Lett*. 2016; 65(1):23.

47. Bočan J, Maňák J, Jäger A. Anisotropic mechanical properties of pure magnesium analyzed by in situ nanoindentation. *Key Eng Mater.* 2015;662:11-14.

SUPPORTING INFORMATION

Additional supporting information may be found in the online version of the article at the publisher's website.

How to cite this article: Hübler D, Winkler K, Riedel R, Kamrani S, Fleck C. Cyclic deformation behavior of Mg–SiC nanocomposites on the macroscale and nanoscale. *Fatigue Fract Eng Mater Struct.* 2022;45(2):386-399. doi:10.1111/ffe.13600